Supplemental Material

A molecular biomarker for end-Permian plant extinction in South China

Chunjiang Wang and Henk Visscher

SAMPLES

The analyzed samples originate from the Permian–Triassic boundary sections exposed near Meishan, Changxing County, Province of Zhejiang, southeastern China (Yin et. al., 2001). For this study, 88 fresh outcrop samples were selected from sections B, C and D. The position of samples from adjacent sections B and C was correlated to Section D (31.0798°N, 119.7058°E), following standardized bed numbering (Yin et al., 2001; Jin et al., 2006; Zhang et al., 2007). For details regarding sample location and lithology see Table S1.

ANALYTICAL METHODS

Organic analysis was performed at the State Key Laboratory of Petroleum Resources and Prospecting and the State Key Laboratory of Heavy Oil Processing, China University of Petroleum (Beijing), under standard organic-geochemical operating methods and procedures. The obtained analytic dataset is made available in Table S1. Data for DBFs/Aros index, moretane/hopane index and $\delta^{13}C_{org}$ partly from earlier studies (Wang and Visscher, 2007; Wang, 2007).

Kerogen preparation. Pre-extracted rock powder was digested by HCl (6N) for 2 h and then by HF (40%) for 2 h at 60–70 °C several times. Acid resistant minerals were removed by floatation using Zn + HCl (6 g/ml). The kerogen concentrate was washed with distilled water, then freeze-dried at –5 ºC for 6 h and finally oven-dried in vacuum at 60 °C for 72 h. Finally, the concentrate was ultrasonication-extracted twice in dichloromethane/methanol (9:1 v/v) for 10 min to remove hydrocarbon residual trapped in the kerogen. The kerogen samples were dried in vacuum at 60 °C prior to Py–GC–MS, elemental, and carbon isotopic analysis.

Extraction and fractionation. The powdered samples (100g–750 g) were Soxhlet-extracted with solvent mixture of dichloromethane/methanol (93:7 v/v) (usually 150 ml), and the extracts were separated into maltenes and asphaltene fractions by precipitating asphaltenes in heptanes. The maltenes were further fractionated into saturate, aromatic and polar fractions by using silica-alumna column chromatography, with hexane, dichloromethane/hexane (2:1 v/v), and dichloromethane/ alcohol (9:1 v/v) as elution solvents, respectively.

TOC and HI measurement. The content of organic carbon for whole rock samples (TOC) was measured using the Leco-WR-112 and CS230HC Carbon Detector. The precision for the TOC measurement is ±1% of the carbon present. The Hydrogen Index (HI) was determined using the OGE-II Rock-Eval System. The precision for the HI measurement ranges from ≤10% for S_2 values >3 mg/g rock to as much as 50% for S_2 values of <0.1 mg/g rock. Beds 23–32 contain Type-III kerogen with

low Rock-Eval hydrogen indices (30–98 mg hydrocarbons/g TOC; see Table S1), confirming predominant terrigenous source material.

Organic-carbon isotope analysis. Organic-carbon isotopic ratios were measured on kerogen using a Thermo Finnigan MAT 253 isotope mass spectrometer interfaced to a Flash EA 2000 elemental analyzer, by a ConFlo IV universal continuous flow interface. The oven-dried kerogen (5–10 mg) was wrapped in a tin capsule. The EA combustion furnace was set to 950 °C. Carbon-isotope delta values ($\delta^{13}C_{org}$) are reported relative to VPDB and calculated using two isotopic standards, namely USGS 24 ($\delta^{13}C$=−16.0‰) and IAEA-600 ($\delta^{13}C$=−24.8‰).

GC–MS analysis. The samples were analyzed using an Agilent 7890-5975c GC–MS equipped with a HP-5MS fused silica capillary column (60 m × 0.25 mm × 0.25 μm). The ion source was operated in EI mode with 70 eV ionization energy and 1200V acceleration voltage at 250 °C. The gas chromatograph was programmed to an initial period of 1 min at 50 °C, then the oven was heated to 120 °C at 20 °C/min, further to 250 °C at 4 °C/min, and finally to 310 °C at 3 °C/min, followed by an isothermal period of 30 min.

Py–GC–MS analysis. A Py–GC–MS system was equipped with a CDS Pyroprobe 5000 series coupled to the Agilent 7890-5975c GC–MS with a CDS1500 valve interface held at 280 °C. A glass tube containing an aliquot of the kerogen was put in a platinum wire loop and heated at 250 °C for 5 s and then programmed to 610 °C at a rate of 20 °C/ms, and the kerogen sample was held at this temperature for 12 s in a flow of helium (99.999%). The GC–MS analysis method is described above.

BIOMARKER QUANTIFICATION

The relative abundance of mono-aromatic *des*-A-oleanane, defined as the MADAO/*n*-alkanes ratio, was calculated by using the peak area of the mono-aromatic *des*-A-oleanane in the *m/z* 159 mass chromatogram and the peak area of *n*-C_{17} + *n*-C_{18} (*m/z* 85) extracted from the GC–MS data of the saturate fractions. For the phenol index, the phenols/*n*-alka(e)nes ratio, defined as C_0–C_2 phenols/C_8–C_{21} (*n*-alkanes + *n*-alkenes), was calculated by using the total peak area of C_0–C_2 phenols (*m/z* 94 + 108 + 122) and that of C_8–C_{21} *n*-alkanes (*m/z* 85) and C_8–C_{21} *n*-alkenes (*m/z* 97) from the Py–GC–MS analysis, while the phenols and *n*-alka(e)nes were quantified by peak height from the Py–GC analysis. The DBFs/Aros index, defined as dibenzofurans/total aromatics ratio, was calculated using the total peak area of C_0–C_1 isomers of dibenzofurans (*m/z* 168 + 182) and that of naphthalenes + phenanthrenes + fluoranthenes + pyrenes + chrysenes + benzofluoranthenes + benzopyrenes + fluorenes + dibenzofurans + dibenzothiophenes (*m/z* 128 + 142 + 178 + 192 + 166 + 180 + 168 + 182 + 184 + 198 + 202 + 216 + 228 + 242 + 252 + 266) from the aromatic GC–MS analysis. The moretane/hopane index describes the ratio of βα-hopanes (moretanes) to αβ-hopanes. All calculated ratios are listed in Table S1.

MADAO IDENTIFICATION

The mass spectra of compounds **1(a,b)** and **2** (main text Fig. 1B) exhibit molecular ion peaks (M^+) at *m/z* 310 and *m/z* 324, corresponding to an elemental composition of $C_{23}H_{34}$ and $C_{24}H_{36}$, respectively. The *m/z* molecular ions, the base peak ions at *m/z* 145 and *m/z* 159, as well as all other corresponding fragment ions of the two compounds are mutually different in mass by 14 amu (atomic mass units), indicative of the substitution of a methyl group by hydrogen. Evidently, the compounds are homologues, sharing identical fragmentation. The presence of a base peak at *m/z* 145 or *m/z* 159 is commonly considered to be diagnostic of mono-aromatic terpenoid hydrocarbons (Hazai et al., 1986; Wolff et al., 1989; Stout, 1992; Ten Haven et al., 1992; Asahi and Sawada, 2019), including C_{23} and C_{24} monoaromatic A-ring degraded pentacyclic triterpenoids derived from either oleanane or ursane precursors. Sedimentary records of such *des*-A-triterpenoids are relatively uncommon. Cenozoic records correspond to an angiosperm derivation, but a gymnospermous – probably bennettitalean (cf.

Taylor et al., 2006) – source should explain the finding of a series of mono-aromatic *des*-A-oleanadienes in Jurassic coal (Wang and Xia, 1995). In general, mass spectral interpretation of the hydrocarbons concerned show fragmentation patterns distinctly different from those of the Meishan compounds **1** and **2**. Differences are well exemplified by spectra of C_{23} and C_{24} mono-aromatic *des*-A-oleanane/ursane-type hydrocarbons, including some isomers of compound **1**, detected in the Oligocene Brandon Lignite, Vermont, USA (Stout, 1992). We know of only one published mass spectrum of an angiospermous C_{23} mono-aromatic tetracyclic compound, which is very similar to that of **1a** and **1b**. Showing a molecular ion at m/z 310, a base peak at *m/z* 145, and characteristic fragments at *m/z* 157, *m/z* 171 and *m/z* 295, this compound – identified as mono-aromatic *des*-A-ursane/oleanane – is part of a series of pentacyclic-triterpenoid derivatives recorded from Miocene turbidites and Holocene tsunami deposits on Hokkaido, Japan, that contain abundant land-plant debris (Asahi and Sawada, 2019).

Observations and experiments indicate that A-ring degradation can already be initiated prior to leaf shedding by the formation of ring-opened (*seco*-) derivatives from triterpenoid C-3 ketones, such as β-amyrone (Baas, 1985; Simoneit et al., 2009), probably through photochemical rather than microbial mediation (Corbet et al., 1980; Simoneit et al., 2009). A-ring cleavage is followed by diagenetic loss of side-chains, and progressive aromatization from ring B towards ring D (Trendel et al., 1989; Lohmann et al., 1990; Stout, 1992; He et al., 2018; Asahi and Sawada, 2019).

Supplemental analysis. Because of the limited published information on C_{23} and C_{24} mono-aromatic *des*-A-oleanane/ursane-type hydrocarbons, we analyzed some drill-core samples from Oligocene coal-bearing deposits in order to ascertain that the Meishan compounds were derived from oleanane, rather than the isomeric ursane skeleton (Fig S1).

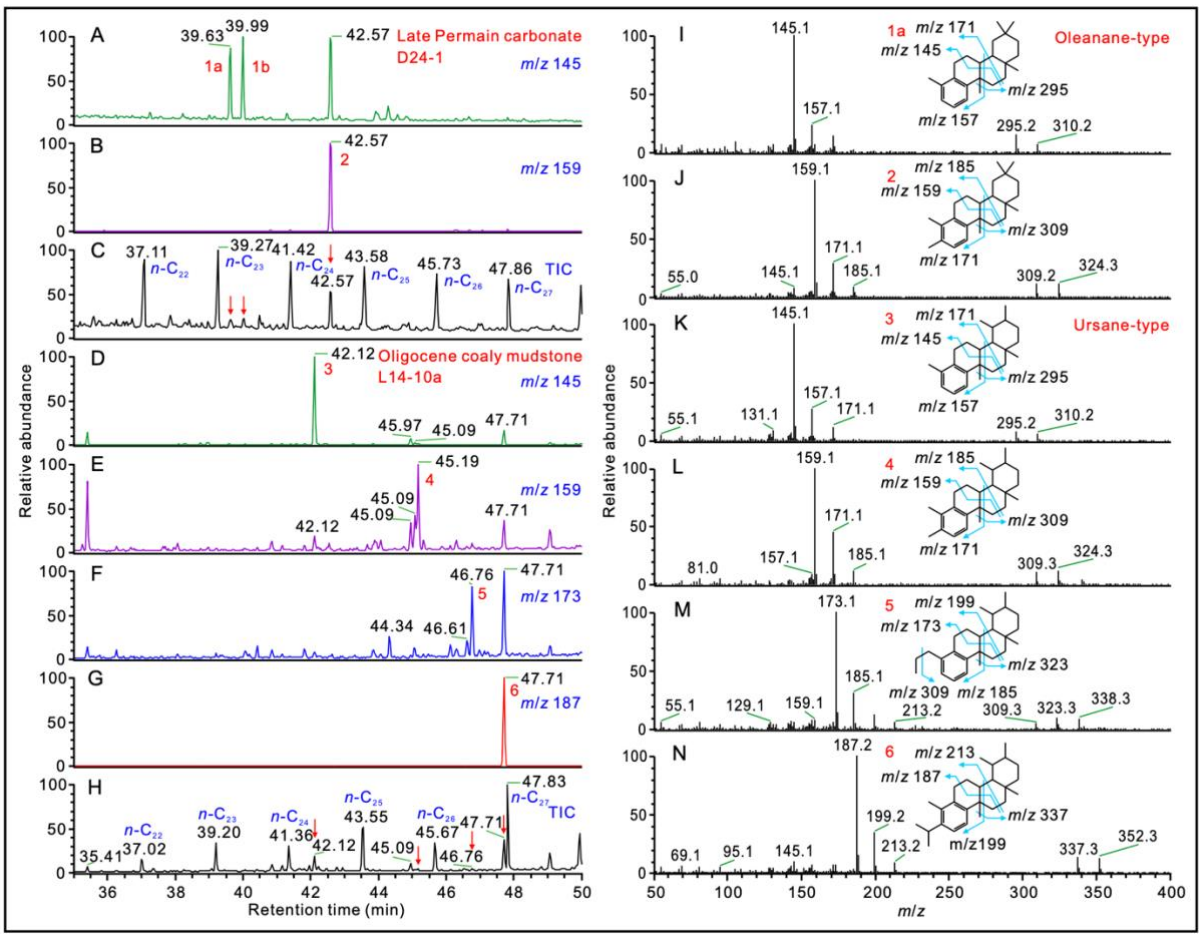

Figure S1. Identification and comparison of mono-aromatic *des*-A-oleanane (MADAO) and mono-aromatic *des*-A-ursane (MADAU). For interpretation of mass chromatograms (A–H) and mass spectra (I–N) see text.

The analyzed samples originate from the Baigang Formation of the Baise Basin (Zhao et al., 1990), Guangxi, southern China. Wetland vegetation was dominated by angiosperms (Li et al., 2019). The samples represent immature coal and coaly mudstone (vitrinite reflectance 0.35%–0.45%), characterized by high TOC (6.2%–53.3%) and high pristane/phytane ratios (4.8–11.3). The organic molecular assemblage preserves a diverse series of pentacyclic triterpenoids and their derivatives. We here focus on a comparative analysis – under the same GC–MS operating conditions – of mono-aromatic *des*-A-oleanane/ursane compounds from the Late Permian Changxing Formation at Meishan and the Oligocene Baigang Formation that could provide robust support to the identification of gigantopterid MADAO.

In Fig. S1, A and B are *m/z* 145 and *m/z* 159 mass chromatograms of a Permian carbonate sample, while D and E are *m/z* 145 and *m/z* 159 mass chromatograms of Oligocene coaly mudstone. It is clear that the eluting times of compounds **3** and **4** are later than those of compounds **1a** and **2**. In I and K, the mass spectra of isomeric compounds **1a** and **3** (C_{23}, MW=310) are very similar, while in J and L, compounds **2** and **4** (C_{24}, MW=324) have similar spectra as well. In general, ursane-type compounds are known to elute significantly later than their oleanane-type isomers (Wolff et al., 1989; Killops et al., 1995). We therefore interpret compounds **1a** and **2** as *des*-A-oleananes, and compounds **3** and **4** as *des*-A-ursanes.

F and G are *m/z* 173 and *m/z* 187 mass chromatograms, showing the eluting times of compounds **5** and **6**. These compounds can be interpretated as C_{25} and C_{26} *des*-A-ursane, based on the mass spectra of M and N, respectively. The four compounds **3**, **4**, **5** and **6** share the same fragmentation pattern, as evidenced by five series of homologous fragment ions, differing by successive 14-amu increments (*m/z* 145-159-173-187, *m/z* 157-171-185-199, *m/z* 171-185-199-213, *m/z* 295-309-323-337, *m/z* 131-145-159-173). The compounds elucidate the *des*-A-oleanane/ursane tetracyclic skeleton with various alkyl-substitutes at the B-ring. The *m/z* 309 (M^+-29) fragment of compound **5** indicates an *n*-propyl group at position C-10, while an *iso*-propyl group attached at C-5 may be the only possible interpretation for the structure of compound **6**. The detection and identification of these alkyl-substituted *des*-A-oleananes/ursanes may well support the proposed pathways leading to the formation of gigantopterid MADAO compounds (main text Fig. 1C).

MARATTIALEAN WETLAND FORESTS

We assume that the above- and below-ground biomass of the Changhsingian wetland forests of South China were greatly dominated by marattialean tree ferns. Anatomically preserved stem remains (e.g., *Psaronius* spp.), abundant foliage (e.g., *Pecopteris*, *Fascipteris* spp.) and occasional fertile fronds (e.g., *Scolecopteris* spp.) are diagnostic of the extinct family Psaroniaceae (Rothwell et al., 2018). The general morphology of the monolete spores of this family is highly variable. Even within a single sporangium, different spore genera can be frequently observed (e.g., *Torispora*, *Thymospora*, *Punctatosporites*, *Laevigatosporites*) (Brousmiche et al., 1992; Lesnikowska and Willard, 1997; Bek, 2021). Together, species of these palynological taxa can compose up to 60% of the parauthochtonous spore/pollen assemblages from the coal-bearing Xuanwei Formation of southwestern China (Ouyang, 1986).

Much like modern tree ferns, the Permian Psaroniaceae lacked secondary xylem (wood). Growing up to 15 meters, false stems were formed by a central upright growing aerial rhizome embedded in a massive mantle composed of a large number of adventitious roots (Morgan, 1959). Anatomically preserved *Psaronius* stems from South China reveal the primary-xylem conduits of the mantle, built up by exceptionally wide tracheids, even up to 250 µm in diameter, with dense scalariform (ladder-like) pitting (e.g., He et al., 2008; D'Rozario et al., 2011). These anatomical traits

testify to highly efficient water conductance from soil to sites of photosynthesis (Brodersen et al., 2014; Olson et al., 2018), enabling tree growth of the non-woody marattialean ferns. The trade-off, however, was the high vulnerability of the trees to fatal drought-induced cavitation and spread of conduction-blocking embolisms. As a consequence, favorable habitats were determined primarily by high year-round soil-moisture availability. Increasing end-Permian rarity and last-occurrences of psaroniaceous fossils in the Kayitou Formation of southwestern China (e.g., Ouyang, 1986; Yu et al., 2015; Chu et al., 2016; Feng et al., 2020) affirm progressive habitat contraction following harshening conditions of periodical soil aridity, on account of a negative soil-water balance (i.e., water input < water output). The transient co-existence of residual wetland forest communities – likely representing wet spots (cf. DiMichele et al., 2006) – with the colonizing drought-adapted *Germaropteris*–*Lepacyclotes* flora implies that end-Permian floral turnover in South China had already started before the ultimate demise of the Psaroniaceae and other consituents of the *Gigantopteris* flora.

REFERENCES

Asahi, H., and Sawada, K., 2019, GC–MS analyses of ring degraded triterpenoids in event deposits: Researches in Organic Geochemistry, v. 35, p. 55−72, https://doi.org/10.20612/rog.35.2_55.

Baas, W.J., 1985, Naturally occurring *seco*-ring-A-triterpenoids and their possible biological significance: Phytochemistry, v. 24, p. 1875–1889, https://doi.org/10.1016/S0031-9422(00)83085-X.

Bek, J., 2021, Palynological grouping of Paleozoic marattialean miospores: Review of Palaeobotany and Palynology, v. 284, 104341, https://doi.org/10.1016/j.revpalbo.2020.104341.

Brodersen, C., Jansen, S., Choat, B., Rico, C., and Pittermann, J., 2014, Cavitation resistance in seedless vascular plants: The structure and function of interconduit pit membranes. Plant Physiology, v. 165, p. 895–904, https://doi.org/10.1104/pp.113.226522.

Brousmiche, C., Coquel, R., and Wagner, R.H., 1992, Les *Scolecopteris* du Stéphanien supérieur du Bassin de Puertollano (Espagne): Geobios, v. 25, p. 323–329, https://doi.org/10.1016/0016-6995(92)80003-V.

Chu, D., Yu, J., Tong, J., Benton, M.J., Song, H., Huang, Y., Song, T., and Tian, L., 2016, Biostratigraphic correlation and mass extinction during the Permian–Triassic transition in continental-marine siliciclastic settings of South China: Global and Planetary Change, v. 146, p. 67–88, https://doi.org/10.1016/j.gloplacha.2016.09.009.

Corbet, B., Albrecht, P., and Ourisson, G., 1980, Photochemical or photomimetic fossil triterpenoids in sediments and petroleum: Journal of the American Chemical Society, v. 102, p. 1171–1173, https://doi.org/10.1021/ja00523a048.

DiMichele, W.A., Tabor, N.J., Chaney, D.S., and Nelson, W.J., 2006, From wetlands to wet spots: Environmental tracking and the fate of Carboniferous elements in Early Permian tropical floras: Geological Society of America Special Paper, v. 399, p. 223–248, https://doi.org/10.1130/2006.2399(11).

D'Rozario, A., Sun, B., Galtier, J., Wang, S.-J., Guo, W.-Y., Yao, Y.-F., and Li, C.-S., 2011, Studies on the Late Permian permineralized tree fern *Psaronius housuoensis* sp. nov. from Yunnan Province, Southwest China: Review of Palaeobotany and Palynology, v. 163, p. 247–263, https://doi.org/10.1016/j.revpalbo.2010.11.002.

Feng, Z., Wei. H.-B., Guo, Y., He., X.-Y., Sui, Q., Zhou, Y., Liu, H.-Y., Gou, X.-D., and Lv, Y., 2020, From rainforest to herbland: New insights into land plant responses to the end-Permian mass extinction: Earth-Science Reviews, v. 204, 103153, https://doi.org/10.1016/j.earscirev.2020.103153.

Hazai, I., Alexander, G., Székely, T., Essiger, B., and Radek, D., 1986, Investigation of hydrocarbon constituents of a young sub-bituminous coal by gas chromatography–mass spectrometry:

Journal of Chromatography, v. 367, p. 117–133, http://doi.org/10.1016/S0021-9673(00)94821-0.

He, D., Simoneit, B.R.T., Cloutier, J.B., and Jaffé, R., 2018, Early diagenesis of triterpenoids derived from mangroves in a subtropical estuary: Organic Geochemistry, v. 125, p. 196–211, https://doi.org/10.1016/j.orggeochem.2018.09.005.

He, X.-Y., Wang, S.J., Hilton, J., Tian, B.-L., and Zhou, Y.-L., 2008, Anatomically preserved marattialean plants from the Upper Permian of southwestern China: The trunk of *Psaronius panxianensis* sp. nov.: Plant Systematics and Evolution, v. 272, p. 155–180, https://doi.org/10.1007/s00606-007-0638-7.

Jin, Y., Wang, Y., Henderson, C., Wardlaw, B.R., Shen, S., and Cao, C., 2006, The Global Boundary Stratotype Section and Point (GSSP) for the base of Changhsingian Stage (Upper Permian): Episodes, v. 29, p. 175–182, https://doi.org/10.18814/epiiugs/2006/v29i3/003.

Killops, S.D., Raine, J.I., Woolhouse, A.D., and Weston, R.J., 1995, Chemostratigraphic evidence of higher plant evolution in the Taranaki Basin, New Zealand: Organic Geochemistry, v. 23, p. 429–445, http://doi.org/10.1016/0146-6380(95)00019-B.

Lesnikowska, A.D., and Willard, D.A., 1997, Two new species of *Scolecopteris* (Marattiales), sources of *Torispora securis* Balme and *Thymospora thiessenii* (Kosanke) Wilson and Venkatachala: Review of Palaeobotany and Palynology, v. 95, p. 211–225, https://doi.org/10.1016/S0034-6667(96)00035-8.

Li, Q., Su, T., Liu, Y., and Quan, C., 2019, Oligocene plant ecological strategies in low-latitude Asia unraveled by leaf economics: Journal of Asian Earth Sciences, v. 182, 103933, https://doi.org/10.1016/j.jseaes.2019.103933.

Lohmann, F., Trendel, J.M., Hetru, C., and Albrecht, P., 1990, C-29 tritiated β-amyrin: chemical synthesis aiming at the study of aromatization processes in sediments: Journal of Labelled Compounds and Radiopharmaceuticals, v. 28, 377–386, https://doi.org/10.1002/jlcr.2580280403.

Morgan, J., 1959, The morphology and anatomy of American species of *Psaronius*: Illinois Biological Monographs, v. 27, p. 1-107, https://doi.org/10.5962/bhl.title.50285.

Olson, M.E., et al., 2018, Plant height and hydraulic vulnerability to drought and cold: Proceedings of the National Academy of Sciences of the United States of America, v. 115, p. 7551–7556, https://doi.org/10.1073/pnas.1721728115.

Ouyang, S., 1986., Palynology of Upper Permian and Lower Triassic strata of Fuyuan district, Eastern Yunnan: Palaeontologia Sinica, New Series A, v. 9, p. 1–122.

Rothwell, G.W., Millay, M.A., and Stockey, R.A., 2018, *Escapia* gen. nov.: Morphological evolution, paleogeographic diversification, and the environmental distribution of marattialean ferns through time, *in* Krings, M., et al., eds., Transformative paleobotany: London, Academic Press, p. 271–360, https://doi.org/10.1016/B978-0-12-813012-4.00014-0.

Simoneit, B.R.T., Xu, Y., Neto, R.R., Cloutier, J.B., and Jaffé, R., 2009, Photochemical alteration of 3-oxygenated triterpenoids: Implications for the origin of 3,4-*seco*-triterpenoids in sediments: Chemosphere, v. 74, p. 543–550, https://doi.org/10.1016/j.chemosphere.2008.09.080.

Stout, S.A., 1992, Aliphatic and aromatic triterpenoid hydrocarbons in a Tertiary angiospermous lignite: Organic Geochemistry, v. 18, p. 51–66, https://doi.org/10.1016/0146-6380(92)90143-L.

Taylor, D.W., Li, H., Dahl, J., Fago, F.J., Zinniker, D., and Moldowan, J.M., 2006, Biogeochemical evidence for the presence of the angiosperm molecular fossil oleanane in Paleozoic and Mesozoic non-angiospermous fossils: Paleobiology, v. 32, p. 179–190, https://doi.org/10.1666/0094-8373(2006)32%5B179:BEFTPO%5D2.0.CO;2.

Ten Haven, H.L., Peakman, T.M. and Rullkötter, J., 1992, Early diagenetic transformation of higher-plant triterpenoids in deep-sea sediments from Baffin Bay: Geochimica et Cosmochimica Acta, v. 56, p. 2001–2024, http://doi.org/10.1016/0016-7037(92)90326-E.

Trendel, J.M., Lohmann, F., Kintzinger, J.P., Albrecht, P., Chiarone, A., Riche, C., Cesario, M., Guilhem, J., and Pascard, C., 1989, Identification of *des*-A-triterpenoid hydrocarbons occurring in surface sediments: Tetrahedron, v. 45, p. 4457–4470, https://doi.org/10.1016/S0040-4020(01)89081-5.

Wang, C., 2007, Anomalous hopane distributions at the Permian–Triassic boundary, Meishan, China – Evidence for the end-Permian marine ecosystem collapse: Organic Geochemistry, v. 38, p. 52–66, https://doi.org/10.1016/j.orggeochem.2006.08.014.

Wang, C., and Visscher, H., 2007, Abundance anomalies of aromatic biomarkers in the Permian–Triassic boundary section at Meishan, China – Evidence of end-Permian terrestrial ecosystem collapse: Palaeogeography, Palaeoclimatology, Palaeoecology, v. 252, p. 291–303, https://doi.org/10.1016/j.palaeo.2006.11.048.

Wang, C., and Xia, Y., 1995, *Des*-A-triterpenoid hydrocarbons in Jurassic coals from the Turpan–Hami Basin: Acta Sedimentologica Sinica, v. 13 (supplement), p. 138–146.

Wolff, G.A., Trendel, J.M., and Albrecht, P., 1989, Novel monoaromatic triterpenoid hydrocarbons occurring in sediments: Tetrahedron, v. 45, p. 6721–6728, https://doi.org/10.1016/S0040-4020(01)89142-0.

Yin, H., Zhang, K., Tong, J., Yang, Z., and Wu, S., 2001, The Global Stratotype Section and Point (GSSP) of the Permian–Triassic boundary: Episodes, v. 24, p. 102–114, https://doi.org/10.18814/epiiugs/2001/v24i2/004.

Yu, J., Broutin, J., Chen, Z., Shi, X., Li, H., Chu, D., and Huang, Q., 2015, Vegetation changeover across the Permian–Triassic Boundary in Southwest China: Extinction, survival, recovery and palaeoclimate: A critical review: Earth-Science Reviews, v. 149, p. 202–224, https://doi.org/10.1016/j.earscirev.2015.04.005.

Zhang, K., Tong, J., Shi, G.R., Lai, X., Yu, J., He, W., Peng, Y., and Jin, Y., 2007, Early Triassic conodont–palynological biostratigraphy of the Meishan D Section in Changxing, Zhejiang Province, South China: Palaeogeography, Palaeoclimatology, Palaeoecology, v. 252, p, 4–23, https://doi.org/10.1016/j.palaeo.2006.11.031.

Zhao, S.-Q., Zhong, N., Xiong, B., Simoneit, B.R.T., and Wang, T.-G., 1990, Organic geochemistry and coal petrology of Tertiary brown coal in the Zhoujing mine, Baise Basin, South China: 1. Occurrence and significance of exudatinite: Fuel, v. 69, p. 4–11, https://doi.org/10.1016/0016-2361(90)90251-K.